Experimental study of ion heating and acceleration during magnetic reconnection*

S. C. Hsu,[†,a)] T. A. Carter, G. Fiksel,[b)] H. Ji, R. M. Kulsrud, and M. Yamada
Princeton Plasma Physics Laboratory, P. O. Box 451, Princeton, New Jersey 08543

(Received 23 October 2000; accepted 24 January 2001)

Ion heating and acceleration has been studied in the well-characterized reconnection layer of the Magnetic Reconnection Experiment [M. Yamada *et al.*, Phys. Plasmas **4**, 1936 (1997)]. Ion temperature in the layer rises substantially during null-helicity reconnection in which reconnecting field lines are anti-parallel. The plasma outflow is sub-Alfvénic due to a downstream back pressure. An ion energy balance calculation based on the data and including classical viscous heating indicates that ions are heated largely via nonclassical mechanisms. The T_i rise is much smaller during co-helicity reconnection in which field lines reconnect obliquely. This is consistent with a slower reconnection rate and a smaller resistivity enhancement over the Spitzer value. These observations show that nonclassical dissipation mechanisms can play an important role both in heating the ions and in facilitating the reconnection process. © *2001 American Institute of Physics.* [DOI: 10.1063/1.1356737]

I. INTRODUCTION

Magnetic reconnection,[1] the topological rearrangement and annihilation of magnetic flux in a highly conductive plasma, is thought to play a central role in coronal heating, magnetospheric dynamics, and ''anomalous'' ion heating in reversed-field pinches and spheromaks. Although reconnection is invoked frequently as an ion heating or acceleration mechanism, a detailed understanding of the energy conversion process is still lacking, largely due to the limited accessibility of reconnection events in both naturally occurring and laboratory plasmas. Description of the process is often limited to ''black box'' phenomenology, in which the input parameters are, for example, implications for magnetic nulls (such as sunspot groups) or measurable magnetic fluctuations (as in RFP's), and the output parameters are energetic particle beams or enhanced global ion heating, respectively. The details of this black box, however, are fundamental to plasma physics since reconnection is a virtually unavoidable process in all magnetized plasmas. Because *local* reconnection changes *global* magnetic field topology, overall plasma equilibrium and confinement properties can be profoundly affected. A well-known example of this is the interaction of the solar wind with the Earth's magnetosphere, in which reconnection along the day-side magnetopause and the polar cusp regions allow solar wind plasma to penetrate into the magnetospheric cavity, occasionally leading to large-scale geomagnetic storms. Detailed understanding of the magnetic energy conversion process could also be the first step toward eventual creative application of such understanding to alternative concept fusion or the minimization and control of confinement-degrading effects in tokamak plasmas.

Recent research on the Magnetic Reconnection Experiment[2] (MRX) has focused on ion heating and acceleration during magnetic reconnection.[3,4] Using a novel spectroscopy probe[5] developed at the University of Wisconsin–Madison, local ion temperature was measured in the well-characterized two-dimensional (2D), quasi-steady-state reconnection layer of MRX. Important questions addressed in this work include: (1) whether ions are heated by reconnection, (2) whether energetic plasma flows develop, (3) what fraction of the dissipated magnetic energy is converted to ion energy, and (4) what is the nature of the energy conversion mechanism(s). It is found that ion temperature T_i rises by a factor of 3 in the reconnection layer during null-helicity reconnection (negligible out-of-plane field) and, furthermore, that the T_i rise is causally linked to the reconnection process. The well-known Alfvénic plasma outflows of classical magnetohydrodynamic (MHD) reconnection models[6] are not observed in MRX due to a downstream back-pressure. An ion energy balance calculation, based on experimental data and including classical viscous heating by the sub-Alfvénic flows, indicates that most of the ion heating occurs via nonclassical mechanisms. Here, ''nonclassical'' is defined as something other than classical Coulomb interactions with ohmically heated electrons or classical viscous interactions with energetic flows, and can include, for example, turbulent wave-particle interactions[7] or effects arising from two-fluid Hall dynamics.[8] The T_i rise is much smaller during co-helicity reconnection (finite out-of-plane field), consistent with the slower reconnection rate and a lower value of resistivity enhancement over the classical Spitzer value for co-helicity compared to null-helicity reconnection. It is possible that nonclassical dissipation mechanisms present in the null-helicity case are reduced in the low-beta, co-helicity case. These experimental observations show that

*Paper VI1 3, Bull. Am. Phys. Soc. **45**, 322 (2000).
[†]Invited speaker.
[a)]Present address: Department of Applied Physics, California Institute of Technology, Pasadena, California 91125. Electronic mail: scotthsu@caltech.edu
[b)]Permanent address: Department of Physics, University of Wisconsin, Madison, Wisconsin 53706.

nonclassical dissipation mechanisms can play an important role both in heating ions and in facilitating the reconnection process.

It is important to note that prior to this work, local T_i measurements had not been made in conjunction with well-characterized reconnection events, although correlations between reconnection and global ion heating as well as energetic ion flows have been reported on TS-3 at the University of Tokyo[9] and on SSX (Swarthmore Spheromak Experiment).[10] In the prior experiments, reconnection was generated by colliding two spheromaks together at a substantial fraction of the Alfvén speed. Possible strong compressional heating during the collision could complicate the interpretation of any observed ion heating and acceleration. The slow formation scheme of MRX allows a quasi-steady-state reconnection layer to form, with magnetic energy dissipation being the dominant heating source. The other main distinction between the present work and prior experiments is the direct local measurement of the majority ion temperature. Prior results were based on line-of-sight averaged neutral and impurity emission[9] or ion flux at the vacuum wall.[10]

This paper is organized as follows. Section II describes the experimental setup, plasma formation and configurations, and diagnostics. Section III presents T_i measurements which show a rise in T_i that is causally linked to reconnection, both temporally and spatially. In this section, it is also shown that the T_i rise is much smaller for co-helicity compared to null-helicity reconnection. Section IV presents measurements of both downstream and toroidal ion flow, showing that flows which develop in either direction are sub-Alfvénic in magnitude (within measurement resolution). Based on the experimental data, an ion energy balance is calculated in Sec. V, showing that classical viscous heating by the flows is small and that the ions are heated predominantly due to nonclassical mechanisms. Section VI discusses the relationship between ion heating and resistivity enhancement and provides a discussion on the possible nonclassical ion heating mechanisms. The paper concludes with a summary.

II. EXPERIMENTAL APPARATUS

Experiments were performed on MRX[2] which produces plasmas satisfying the MHD criteria globally ($S \gg 1$, $\rho_i \ll L$, $V_A \ll c$, where S is the Lundquist number, ρ_i the ion gyroradius, L the characteristic length of the reconnection layer, V_A the Alfvén speed, and c the speed of light). Formation and control of the reconnection layer in MRX is unique among laboratory experiments. ''Flux-cores'' containing toroidal field (TF) and poloidal field (PF) coils, shown in Fig. 1(a), allow the controlled formation of a toroidal, axisymmetric reconnection layer, shown schematically in Fig. 1(b). The arrows represent the motion of plasma and magnetic flux during ''pull'' reconnection, in which ''public flux'' linking both flux cores is reconnected into ''private flux'' linking each individual flux core. This sequence produces a reconnection layer elongated in the Z direction which persists for approximately 10 Alfvén transit times ($\tau_A \equiv L/V_A \approx 1.5\ \mu$s). When the TF coils are connected with opposite (same) polarity, the toroidal (out-of-plane) field B_θ is negligible (finite), resulting in null-helicity (co-helicity) reconnection. For more details on the experimental apparatus, please see Ref. 2. Previously, detailed magnetic field measurements from the reconnection layer were reported,[2] revealing Y-shaped (O-shaped) diffusion regions in the null-helicity (co-helicity) case and a neutral sheet half-thickness $\delta \sim c/\omega_{pi} \sim \rho_i \sim 2$cm, where ω_{pi} is the ion plasma frequency. The reconnection rate was found to be consistent with a generalized Sweet–Parker model[11] in which the effects of compressibility, downstream pressure, and nonclassical resistivity are considered. More recently, the profile and thickness of the neutral sheet in MRX was shown[12] to agree with a modified Harris sheet equilibrium.[13]

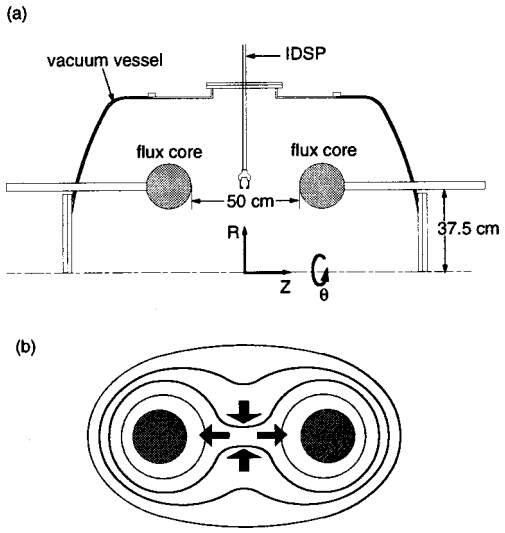

FIG. 1. (a) A schematic of the upper-half plane of MRX, showing the flux cores, position of the IDSP, and the coordinate system. (b) A schematic illustrating motion of plasma and contours of constant poloidal flux and formation of the pull reconnection layer.

In MRX, all three components of the magnetic field vector **B** are measured locally using magnetic probe arrays, and electron density n_e and temperature T_e are measured using a triple Langmuir probe. Other reconnection quantities are inferred from the direct measurements, including the poloidal flux $\psi \equiv \int_0^R 2\pi R' B_Z(R')dR'$ (invoking axisymmetry[14]), reconnection layer current density $j_\theta \approx -(\partial B_Z/\partial R)/\mu_0$, reconnection electric field $E_\theta = -(\partial\psi/\partial t)/2\pi R$, resistivity in the reconnection layer $\eta^* \equiv E_\theta/j_\theta$, Spitzer resistivity $\eta \sim T_e^{-3/2}$, Alfvén speed $V_A \equiv B/\sqrt{\mu_0\rho}$ (using the reconnecting B at the edge of the layer), and plasma inflow speed $V_R \approx -(\partial\psi/\partial t)/(\partial\psi/\partial R)$ (invoking flux-freezing outside the diffusion region). The experiments reported here use pure helium discharges in order to achieve a direct measurement of T_i via Doppler spectroscopy of the He II 4686 Å line. Parameters for the present experiments are as follows: $n_e \approx 5\times10^{13}$ cm^{-3}, $T_e \approx 10-15$ eV, and $T_i \approx 5-15$ eV (all in the reconnection layer), $B \approx 250$ G at the edge of the layer, and $S \equiv \mu_0 L V_A/\eta \approx 250-500$. Qualitative features of the reconnection layer for the present helium discharges are similar to those of previously reported hydrogen discharges,[2] except $\delta_{\mathrm{He}} \approx 2\delta_{\mathrm{H}}$, consistent with the previously reported δ

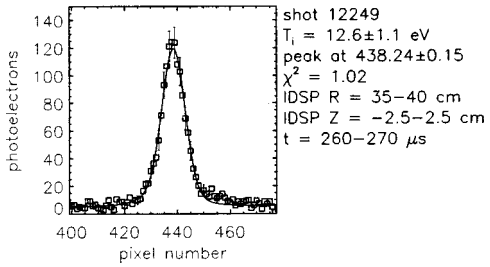

FIG. 2. An example of the He II 4686 Å spectral line, as measured by the IDSP, fitted with a convolution of a Gaussian and the known instrumental broadening.

$\sim\rho_i$ scaling.[2] Spatially, the reconnection region is located in an area given by $R\approx 35\rightarrow 40$ cm and $Z\approx -10\rightarrow 10$ cm.

A major new accomplishment of this work is the local measurement of T_i using the Ion Dynamics Spectroscopy Probe[5] (IDSP) developed at University of Wisconsin–Madison. The IDSP is an insertable probe which collects plasma light from a localized volume. Two perpendicular lines-of-sight (5 cm in length) can give simultaneous Doppler broadening and relative Doppler shift information, although only one line-of-sight is used for the present experiments. Figure 1(b) shows the placement of the IDSP in MRX (to scale); the lines-of-sight can be oriented in an $R-Z$ or $R-\theta$ plane. Further details of the probe are described in Ref. 5. Plasma light is delivered via fiber optics to a 1 m monochromator (0.05 Å resolution) and imaged with a gated charge-coupled device (CCD) camera (wavelength resolution of 0.074 Å /pixel). The reported T_i values are determined by fitting He II 4686 Å spectra to a single Gaussian convolved with the known instrumental broadening, an example of which is shown in Fig. 2. The approximately 0.2 Å of fine structure in this emission line (slightly less than instrumental broadening) introduces a small systematic error (less than 20%) in the lower range of reported T_i values and can be neglected without altering the physics conclusions of the paper. Time resolution is limited by available light, requiring the width of the CCD gate signal to be $\geqslant 10$ μs. Stark broadening is negligible, and IDSP perturbation of the plasma was seen to be minimal after approximately 15 conditioning discharges at the start of each run-day. IDSP Doppler shifts are also used to calibrate[4] Mach probe measurements of ion flow speed derived from an unmagnetized fluid sheath theory[15] generalized for $T_i\approx T_e$ (see the Appendix).

III. IDENTIFICATION OF ION HEATING

A. Time evolution of ion temperature

If ions are heated predominantly by the reconnection process, one might expect T_i to increase with time in the reconnection layer when reconnection is driven and T_i to remain constant when reconnection is not driven, provided that all other controllable parameters are unchanged. However, note that failure to observe a rise in T_i does not preclude ion heating because the observed T_i also depends on the rate of ion heat loss from the volume being sampled.

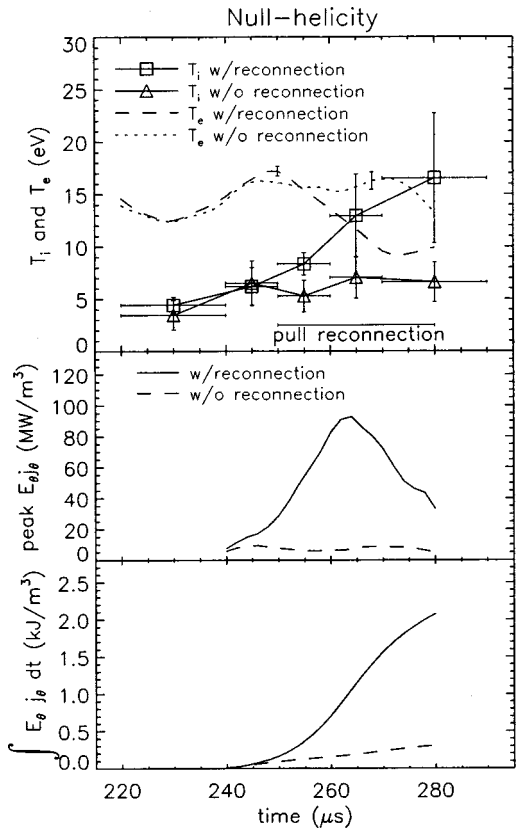

FIG. 3. Time evolution of (top) T_i and T_e, (middle) local heating rate $E_\theta j_\theta$, and (bottom) dissipated magnetic energy $\int_{240\ \mu s}^{t}(E_\theta j_\theta)dt'$ per unit volume, all in the center of the reconnection layer for null-helicity discharges (IDSP located at $R=37.5$ cm and $Z=0$ cm).

With the IDSP situated in the center of the reconnection region ($R=35\rightarrow 40$ cm and $Z=-2.5\rightarrow 2.5$ cm), as shown in Fig. 1(a), T_i as a function of time was obtained for four cases: with and without reconnection for both null-helicity and co-helicity discharges. ''Pull'' reconnection is driven when the PF current is allowed to ramp down after reaching its peak, which induces the requisite E_θ in the plasma from time $t\approx 250\rightarrow 280$ μs. To suppress reconnection, the PF circuit is shorted out (crowbarred) at the approximate time of peak current so that the current decays over several hundred microseconds and the induced E_θ is much smaller. All other controllable parameters, such as capacitor bank voltage and initial gas pressure, were kept constant.[16] The T_i time scan was accomplished by advancing the CCD gate trigger timing over multiple plasma discharges. The CCD gate is open for 10 μs but increased to 20 μs early and late in the scans due to limited plasma light.

1. Null-helicity

A substantial rise in T_i in the center of the reconnection layer, from approximately 6 to 17 eV, is observed when reconnection is driven, and no rise in T_i is observed when reconnection is not driven, as shown in Fig. 3(top) for null-helicity reconnection. The initial $T_i\approx 3-5$ eV before $t\approx 245$ μs for both cases is believed to result from the earlier ''push'' reconnection phase.[17] In Fig. 3(top), error bars in the ordinate represent standard deviations in an ensemble of T_i

measurements (5–10 discharges), and error bars in the abscissa represent the CCD gate time. The rise in T_i is strongly correlated with the magnetic energy dissipation rate, as represented by the value of $E_\theta j_\theta$ in the center of the reconnection layer, shown in Fig. 3(middle). For the case in which no reconnection is driven, the dissipation rate is smaller by a factor of 10, consistent with T_i remaining constant. Taking the time integral of $E_\theta j_\theta$ gives the dissipated magnetic energy per unit volume at the center of the reconnection layer, as shown in Fig. 3(bottom). Note the remarkable agreement in the time evolution of T_i and the dissipated magnetic energy for both cases, but especially for the case with reconnection. These observations indicate strongly that reconnection provides the energy source for the rise in T_i.

The time evolution of T_e is shown in Fig. 3(top). The T_e is already at 15 eV early in the discharge, likely due to ohmic heating associated with plasma formation. The time evolution of T_e starts to diverge around $t \approx 250$ μs for the two cases of with and without reconnection. It might appear counter-intuitive that T_e decreases when reconnection is driven and stays constant when reconnection is not driven. However, a likely explanation is the following. Radiative losses are enhanced due to higher density when reconnection is driven. Thus, even if electrons are heated due to reconnection current sheet dissipation, T_e could decrease if radiated power overwhelms the heating rate. This would be consistent with the T_e data in Fig. 3(top). Another interesting explanation could be the conversion of electron energy to ion energy via nonclassical processes which arise only when reconnection is driven. However, it should be emphasized that a conclusive explanation of the T_e data would require further investigation.

A direct ion heating mechanism must be operative if reconnection is responsible for the ion heating. ''Direct'' means that dissipated field energy is converted to ion energy without requiring classical energy exchange with electrons. In these helium discharges, ions cannot be heated classically by the electrons because the ion-electron energy equipartition time is 400 μs or more, and furthermore, the energy gained by electrons during reconnection due to classical ohmic heating is insufficient by an order of magnitude. One obvious direct ion heating mechanism which would be consistent with the data in Fig. 3 is classical viscous heating by ion flows accelerated during reconnection. However, classical viscous heating is estimated later in Sec. V E to be insufficient in MRX. This leaves only the possibility of nonclassical mechanisms.

2. Co-helicity

In the co-helicity case, T_i also rises during reconnection, from approximately 3 to 7 eV, as shown in Fig. 4(top). Again, no rise in T_i is observed if reconnection is not driven. The local magnetic energy dissipation rate $E_\theta j_\theta$ is shown in Fig. 4(middle). In magnitude, it is on average a factor of 2 smaller than the null-helicity case, consistent with the observed smaller rise in T_i. The dissipated magnetic energy as a function of time is shown in Fig. 4(bottom), and the initial rise in T_i is well correlated with the dissipated magnetic

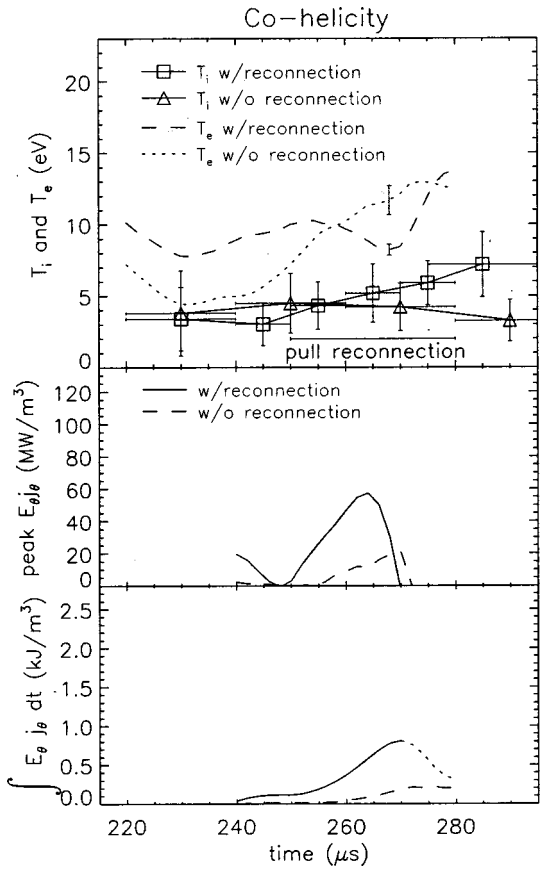

FIG. 4. Time evolution of (top) T_i and T_e, (middle) local heating rate $E_\theta j_\theta$, and (bottom) energy dissipated $\int_{240\ \mu s}^{t}(E_\theta j_\theta)dt'$ per unit volume, all in the center of the reconnection layer for co-helicity discharges (IDSP located at $R=37.5$ cm and $Z=0$ cm). The nonphysical decrease in dissipated energy (represented by the dotted line in the bottom panel) is a result of E_θ going negative due to the plasma ''pinching off'' from one flux core.

energy. The nonphysical dotted section of the curve after $t = 270$ μs is a result of the $E_\theta j_\theta$ term going negative due to the plasma ''pinching off'' from one flux core, and this should not be interpreted as part of the main reconnection sequence. The continued rise in T_i after $t = 270$ μs is likely due to uncontrolled reconnection and the improved confinement associated with the formation of a spheromak-like configuration.

The time evolution of T_e, shown in Fig. 4(top), for the co-helicity case differs from the null-helicity case. First, $T_e \approx 10$ eV for the co-helicity case compared to 15 eV for the null-helicity case. The discussion given previously to account for the difference in T_e after $t \approx 250$ μs for null-helicity should apply to the co-helicity case also, except in this case the T_e rise at $t = 270$ μs (with reconnection) may be due to the improved confinement of the ''pinched-off'' spheromak. The difference in T_e before $t \approx 250$ μs in this case may be attributed to a very early PF crowbar time of $t = 200$ μs for suppressing reconnection (compared to $t = 220$ μs for null-helicity), meaning there is less early heating due to the push[17] reconnection phase for the co-helicity experiments.

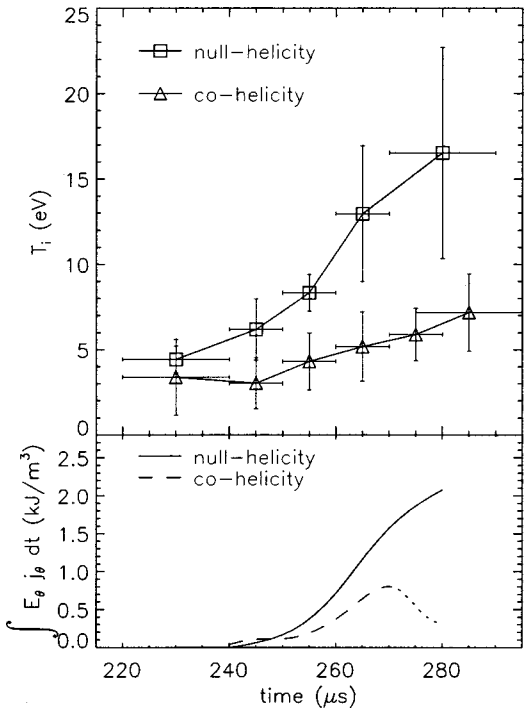

FIG. 5. Time evolution of (top) T_i with the IDSP placed in the center of the reconnection layer ($R=37.5$ cm and $Z=0$ cm) and (bottom) dissipated magnetic energy for both null-helicity and co-helicity reconnection.

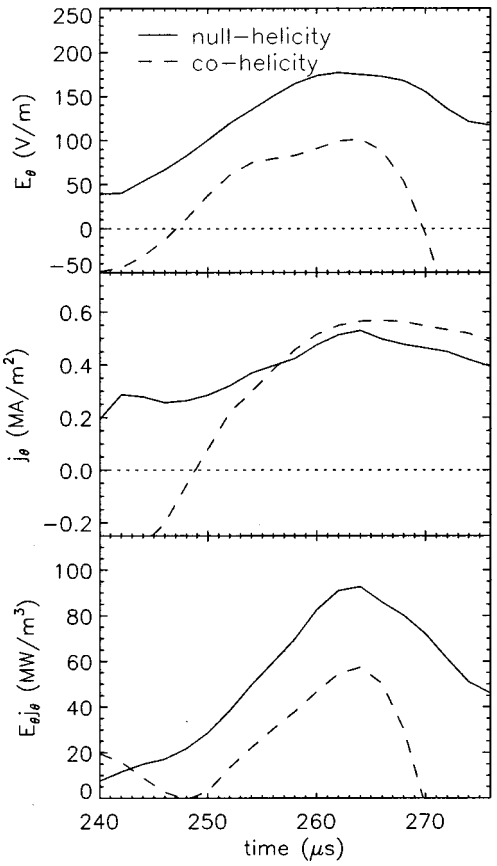

FIG. 6. Time evolution of (top) E_θ, (middle) j_θ, and (bottom) $E_\theta j_\theta$ for null-helicity and co-helicity, all in the center of the reconnection layer.

3. Comparison of null-helicity and co-helicity

Figure 5 shows the key results from null-helicity and co-helicity together. In the null-helicity case, T_i rises by an amount $\Delta T_i \approx 11$ eV (from $t=245\rightarrow 280$ μs) and the local dissipated energy at $t=280$ μs is 2.1 kJ/m^3. In the co-helicity case, which is valid up to $t=270$ μs (due to E_θ going negative), $\Delta T_i \approx 2.5$ eV (from $t=245\rightarrow 270$ μs) and the local dissipated energy is 0.8 kJ/m^3 and $t=270$ μs. These numbers indicate that null-helicity reconnection heats ions more effectively since 2.6 times more dissipated energy resulted in 4.4 times the rise in T_i. Furthermore, the large difference exists despite the fact that co-helicity likely has better ion confinement due to a strong toroidal field.

Stronger ion heating might suggest the increased effect of nonclassical dissipation, and this can be investigated with respect to resistivity enhancement over the classical Spitzer value. Figure 6 shows the time evolution of E_θ and j_θ separately (as well as $E_\theta j_\theta$) for null-helicity and co-helicity reconnection.[18] A time-averaged effective resistivity, $\eta^* \equiv E_\theta / j_\theta$, can be determined for the two cases. For the null-helicity case (averaging over $t\approx 245\rightarrow 280$ μs), $\eta^* \approx (140\,\mathrm{V/m})/(0.4\,\mathrm{MA/m^2}) \approx 3.5\times 10^{-4}$ Ω m and the classical $\eta_\perp \approx 2\times 10^{-5}$ Ω m ($T_e \approx 15$ eV, using $Z_{\mathrm{eff}}=1$) resulting in an enhancement factor of 18. For the co-helicity case (averaging over $t\approx 250\rightarrow 270$ μs), $\eta^* \approx (50\,\mathrm{V/m})/(0.35\,\mathrm{MA/m^2}) \approx 1.4\times 10^{-4}$ Ω m, and the classical $\eta_\parallel \approx 1.8\times 10^{-5}$ Ω m ($T_e \approx 10$ eV, using $Z_{\mathrm{eff}}=1$), resulting in an enhancement factor of 8. Note that η^* is compared to the classical $\eta_\perp$ ($\eta_\parallel$) for cross-field (parallel) current of the null-helicity (co-helicity) case. The larger resistivity enhancement for null-helicity compared to co-helicity is consistent with the implied stronger heating. The reduced dissipation rate in co-helicity is due to a factor of 2 reduction in E_θ, which translates to a slower reconnection speed (since reconnection speed is proportional to E_θ). This is consistent with previous findings that co-helicity reconnection is up to a factor of 3 slower than null-helicity[2] and counter-helicity reconnection.[19]

4. Summary

In these T_i temporal-scan experiments, an increase in T_i during reconnection was identified and causally linked to the presence of reconnection. This is an important result because ion heating due to reconnection had not been identified experimentally before in a rigorous manner. In both null-helicity and co-helicity reconnection, T_i increased when reconnection was driven and stayed constant when reconnection was not driven. The T_i increase correlated well with the dissipation of magnetic energy due to reconnection, showing remarkable proportionality with the dissipated field energy in the null-helicity case. Null-helicity reconnection resulted in a disproportionally higher T_i increase compared to the co-helicity case, indicating stronger ion heating for null-helicity. This is consistent with the fact that null-helicity reconnection had a higher value of resistivity enhancement, which suggests the possible role played by nonclassical dissipation mechanisms.

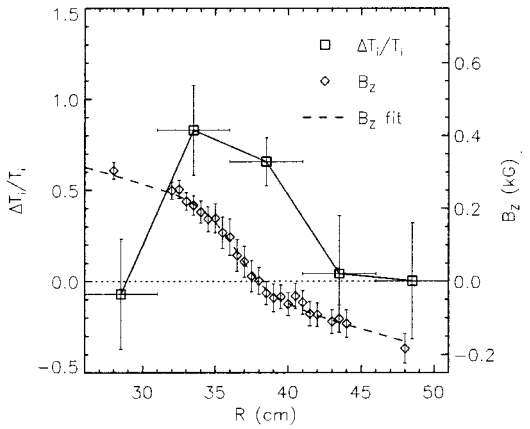

FIG. 7. Radial profiles of (solid line) the relative rise in T_i from $t=255 \rightarrow 265$ μs ($R=37.5$ cm, $Z=0$ cm) and (dashed line) the reconnecting field B_Z during the same time (also at $Z=0$ cm) for null-helicity discharges (shots 11 614–11 659).

B. Radial profile of ion temperature rise

If ions are heated predominantly by the reconnection process, one would also expect the observable rise in T_i to be largest near the reconnection layer ($R \approx 35 \rightarrow 40$ cm). Indeed, this was seen experimentally.

To determine the spatial profile of the ion heating, the IDSP was scanned in R for two CCD gate times, $t_1=250 \rightarrow 260$ μs and $t_2=260 \rightarrow 270$ μs; define $\Delta T_i = T_i(t_2) - T_i(t_1)$. Figure 7 shows a peaked profile for $\Delta T_i / T_i(t_1)$ for null-helicity reconnection, suggesting that ion heating occurred in the vicinity of the reconnection layer. The reconnecting field B_Z profile averaged over the same shots is also shown to indicate the location of the reconnection layer (between the ''knees'' of the B_Z profile, $R \approx 35 \rightarrow 40$ cm). Ion temperature rises approximately 75% in the reconnection layer and not at all elsewhere. Error bars in the ordinate represent one standard deviation in an ensemble of ΔT_i measurements (approximately five discharges at each gate time), and error bars in the abscissa represent the spatial region from which plasma light is collected by the IDSP.

For the co-helicity case, rise in T_i is small compared to the statistical error between shots, and the observed spatial heating profile is essentially flat (within error bars). Better temporal and spatial resolution than what is currently possible is required to reveal a meaningful spatial profile of $\Delta T_i / T_i$ for co-helicity discharges.

In the above experiment, a spatial correlation between the rise in T_i and the location of the reconnection layer was shown. This is further indication that the reconnection process is directly responsible for the observed rise in T_i.

IV. ION FLOW MEASUREMENTS

Reconnection is generally expected to accelerate bulk plasma flows. There is evidence for this in solar observational data, magnetospheric satellite data, and in laboratory experiments. Indeed, reconnection can hardly be mentioned without the expectation of Alfvénic plasma flows. One of the conventionally accepted means of ion heating is via classical viscous damping of these flows. However, measurements of ion flow in MRX suggest that a different scenario is possible, namely that substantial ion heating during reconnection can occur even with sub-Alfvénic flows and small classical viscous heating.

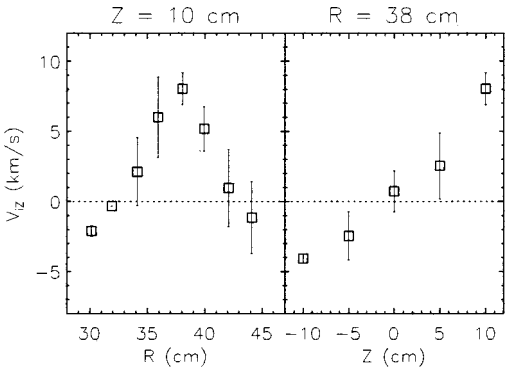

FIG. 8. Mach probe measurements of V_{iZ} as a function of R at $Z=10$ cm and as a function of Z at $R=38$ cm averaged over $t=250 \rightarrow 270$ μs.

A. Downstream flow

Ion downstream flow speed profiles were measured locally using a Mach probe, the data from which was calibrated using the IDSP. The maximum downstream flow $V_{iZ} \approx 8$ km/s, as shown in Fig. 8 for null-helicity reconnection, is equal to $0.2V_A$, where $V_A \approx 39$ km/s ($n_e \approx 5 \times 10^{13}$ cm^{-3}, $B \approx 250$ G, and mass of helium). The flow speed is also seen to increase linearly from 0 to 8 km/s along the layer from $Z=0 \rightarrow 10$ cm. The pattern of the flow is consistent with two-dimensional (2D) theoretical reconnection models, e.g., Sweet–Parker, but the magnitude of the flow differs substantially (theoretical models generally predict downstream flows at the Alfvén speed V_A). Downstream flow for the co-helicity case is similar in profile and magnitude.

The maximum energy density of the measured flow ($\rho V_{iZ}^2/2 \approx 11$ J/m^3, using $n_e = 5 \times 10^{13}$ cm^{-3}) is an order of magnitude smaller than the observed ion thermal energy density increase ($3n\Delta T_i/2 \approx 120$ J/m^3, using $n_e = 5 \times 10^{13}$ cm^{-3} which remains roughly constant in time and $\Delta T_i = 10$ eV), implying that the observed ion heating is unlikely to result from thermalization of the outflow. Furthermore, since the flows are stronger at the edges of the layer ($Z = \pm 10$ cm), ion heating due to viscosity could not easily explain the observed ion heating in the center of the reconnection region ($Z=0$ cm). Estimates of the ion heating due to classical viscosity are estimated in Sec. V E and shown to be small.

The sub-Alfvénic V_{iZ} in MRX is consistent with the buildup of high downstream pressure which reduces the ∇p force along Z.[11] Theoretical models generally assume a low ambient downstream pressure, and thus ion flows can be accelerated to V_A. In MRX, high downstream electron pressure[20] has been verified by Langmuir probe measurements of n_e and T_e in the downstream region. The Z profile of nT_e is peaked near $Z=0$ cm early in the reconnection phase but it becomes flat later in the reconnection phase, mostly due to a rise in n_e.

The absence of energetic downstream flows in MRX is

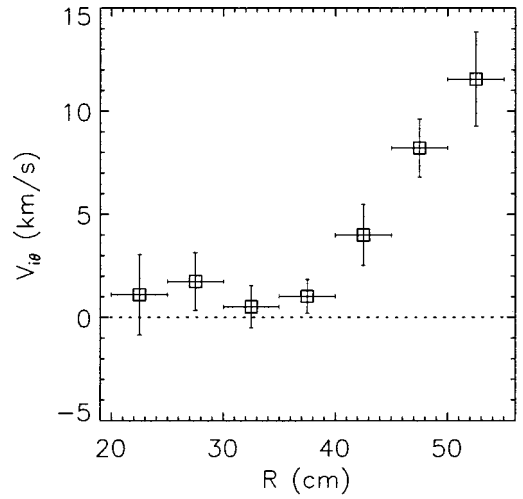

FIG. 9. IDSP measurement of toroidal ion flow $V_{i\theta}$ at $Z=0$ cm and $t=250\rightarrow270$ μs for null-helicity reconnection (shots 10 981–11 097).

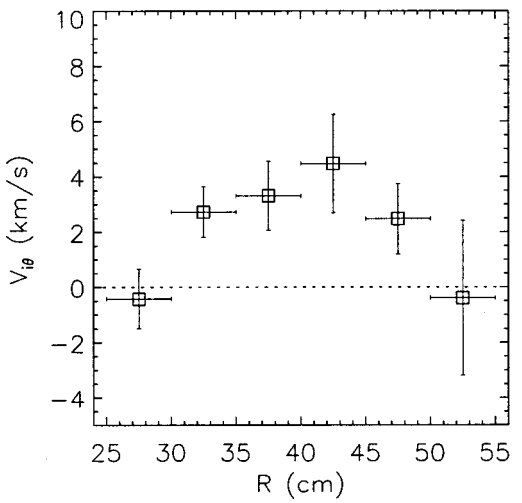

FIG. 10. IDSP measurement of toroidal ion flow $V_{i\theta}$ at $Z=0$ cm and $t=250\rightarrow270$ μs for co-helicity reconnection (shots 11 343–11 428).

an important difference compared to the situations in TS-3[9] and SSX,[10] in which ions are accelerated to V_A. The downstream pressures in TS-3 and SSX were likely to be much lower than the pressures in the reconnection layers. In MRX, ion heating can occur without the development of energetic downstream flows, an important new observation. This effect is also an interesting example of how global boundary conditions can affect the local reconnection dynamics.

B. Out-of-plane flow

Toroidal ion drift speed $V_{i\theta}$ measurements reported here are based on Doppler shifts of the He II 4686 Å ion line emission collected locally by the IDSP. The IDSP is scanned over several radial positions. At each radial position, 5–10 shots are taken with the sightline at a 45° angle to the $+\theta$ direction, and then this is repeated with the sightline at a 45° angle to the $-\theta$ direction. The averaged difference (of course accounting for the angle of the sightlines) gives the relative Doppler shift, which translates to an absolute $V_{i\theta}$. CCD gate time is $t=250\rightarrow270$ μs. It is important to recognize that these measurements have limitations due to spatial (5 cm) and temporal (20 μs) averaging effects, and thus it is conceivable that the local, instantaneous $V_{i\theta}$ might be underestimated. However, Mach probe measurements of $V_{i\theta}$, which yield much better spatial (<1 cm) and temporal (digitized at 2 μs) resolution, show relatively good agreement.

Figure 9 shows the radial profile of $V_{i\theta}$ for null-helicity reconnection. Vertical error bars represent shot-to-shot variation and horizontal error bars represent the spatial extent of the IDSP. The profile shape is somewhat unexpected, but it has been verified many times by different measurements (Mach probe and chord-averaged spectroscopy). Since there is very little current beyond $R=40$ cm, these measurements imply that the entire plasma (not just ions) is rotating on the outside. Most importantly, note that the magnitude of $V_{i\theta}$ in the layer ($R\approx35\rightarrow40$ cm) is much less than the ion thermal speed ($v_{\mathrm{th},i}\equiv\sqrt{2kT_i/m_i}\approx27$ km/s for 15 eV helium ions). The co-helicity case is quite different, as shown in Fig. 10. The flow profile is symmetric and peaked slightly outside the current sheet. The peak value of $V_{i\theta}$ in the layer is higher than for the null-helicity case but still only 5 km/s (<1 eV).

The important conclusion of the toroidal flow measurements is that the observed ion heating does not originate from energetic toroidal ion flows in the layer. The instantaneous energy density of these flows ($\rho V_{i\theta}^2/2\lesssim1.5$ J/m^3) is two orders of magnitude smaller than the observed ion thermal energy density (≈120 J/m^3) and, as in the downstream flow case, classical viscous heating by these flows is insufficient to account for the ion heating, even if $V_{i\theta}$ is indeed underestimated by an order of magnitude; this is shown in Sec. V E.

These measurements imply that ion contribution to the toroidal current is insignificant. In general, the out-of-plane reconnection electric field E_θ is a candidate for particle acceleration to very high energies, especially in collisionless events such as solar flares. In MRX, which has $E_\theta\sim150$ V/m, acceleration of ions to $v_{\mathrm{th},i}\approx27$ km/s would require only 8 μs (if particles are allowed to accelerate unimpeded by magnetic fields). Furthermore, the Harris model,[13] which predicts magnetic field profiles and δ values consistent with MRX,[12] has ions drifting at the diamagnetic speed (≈30 km/s in MRX). Therefore, it is valid to question why larger values of $V_{i\theta}$ are not observed in MRX. A likely reason is the cancellation of any E_θ acceleration by an $E_R\times B_Z$ drift.[21] Other mechanisms which might inhibit E_θ acceleration include Speiser orbit effects,[22] wave-particle scattering,[23] and finite time of ion residence in the current sheet due to reconnection outflow V_{iZ}. The conclusive resolution of these important questions requires further investigation, and it will be obtained only after surveying a much wider parameter regime.

V. ION ENERGY BALANCE DURING RECONNECTION

In this section, an energy balance for ions during null-helicity reconnection is considered in detail. The goal is to determine a lower bound on the energy gained by ions during the reconnection process and to estimate how much of

that energy is converted nonclassically. The energy balance equation used here is based on Eq. (1.23) of Braginskii,[24]

$$\frac{3}{2}\frac{\partial(nT_i)}{\partial t}+nT_i\nabla\cdot\mathbf{V}+\nabla\cdot\left(\frac{3}{2}nT_i\mathbf{V}\right)+\nabla\cdot\mathbf{q} = Q_{i\text{-}n}+\underbrace{Q_{\text{vis}}+Q_{i-e}}_{Q_{\text{classical}}}+Q_{\text{noncl}}, \tag{1}$$

where the terms on the left-hand side (LHS) are (from left to right) rise in ion thermal energy density, a compression term including work done by pressure, convective heat loss, and conductive heat loss. The terms on the right-hand side (RHS) are sinks and sources of energy for the ions, including (from left to right) energy lost to neutrals, viscous heating, heating due to electron-ion collisions, and any nonclassical ion heating mechanisms (e.g., due to wave-particle interactions). The second and third terms on the RHS represent energy due to classical heating. The total ion heating is some fraction of the reconnected field energy, which is known from $E_\theta j_\theta$ derived from magnetic probe measurements. Each term of Eq. (1) will be estimated based on experimental data wherever possible. Note that Q_{i-e} can be neglected since the characteristic classical ion-electron energy equilibration time is more than 400 μs and thus irrelevant on the 30 μs time scale of the reconnection process.

The results show that a substantial fraction (more than half) of the reconnected field energy is converted to ion energy, mostly due to nonclassical mechanisms. These results differ from reported TS-3 results[9] in which ion heating was attributed predominantly to viscous damping of Alfvénic ion flows, and from classical MHD reconnection models in which ions are heated both by viscosity and by energy exchange with ohmically heated electrons.

In calculating an energy balance, a finite volume and time duration must be defined. Here, the energy balance is considered for a given volume $V=5.9\times10^{-3}$ m^3, which is the area monitored by the IDSP ($R=35\rightarrow40$ cm and $Z=-2.5\rightarrow2.5$ cm) revolved around the axis of symmetry. Thus, the volume V is a toroid coinciding with the center of the current sheet. The time duration Δt considered is the pull reconnection phase, $t_1=245\rightarrow t_2=265$ μs. The data are from a set of null-helicity discharges with the same parameters[16] as the ones in Figs. 3 and 7. Note that all the calculations in this section invoke axisymmetry since T_i measurements are known only at one toroidal position.

A. Reconnected field energy

Before examining the terms in Eq. (1), the energy released due to reconnection will be calculated first. The dissipated magnetic field energy can be calculated according to

$$W_{\text{rec}}=\int_{t_1}^{t_2}\int_V \mathbf{E}\cdot\mathbf{j}\,d^3V\,dt\approx\int_{t_1}^{t_2}\int_V E_\theta j_\theta\,\mathrm{d}^3V\,dt, \tag{2}$$

which represents the *total energy due to reconnection* available to heat ions (and electrons). The toroidal electric field E_θ and current density j_θ as a function of R and t are shown in Figs. 11 and 12, respectively.

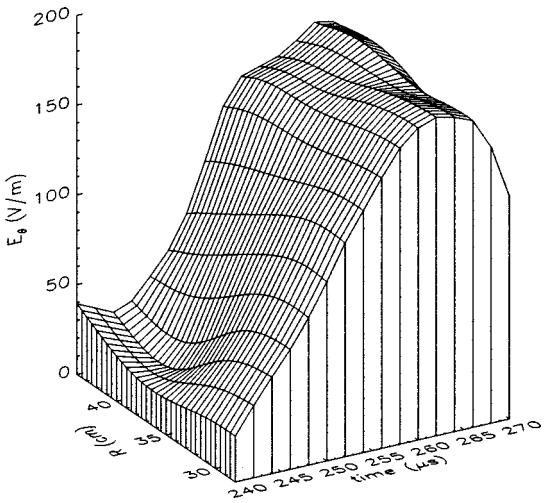

FIG. 11. Surface plot of null-helicity E_θ as a function of radius and time, averaged over $Z=-2.5\rightarrow2.5$ cm (from 90-channel probe measurements, averaged over shots 12 233–12 266).

Note that E_θ is relatively uniform in space, while j_θ is peaked near $R=37$ cm. Both quantities increase in time as pull reconnection proceeds and then reach a short flat-top around $t=260$ μs before starting to decrease. Energy dissipation is clearly strongest in the reconnection layer where j_θ is concentrated. Using the E_θ and j_θ data in Eq. (2) gives $W_{\text{rec}}\approx4.8\pm0.7$ J. It should be noted that the volume V, is only a fraction of the total reconnection volume, and that the total energy dissipated in the entire reconnection volume during Δt is estimated to be on the order of 30 J.

B. Increase in ion thermal energy

The increase in ion thermal energy, the first term on the LHS of Eq. (1), in volume V during reconnection is calculated as follows:

$$\Delta W_{\text{th},i}\equiv\tfrac{3}{2}[\overline{n}(t_2)T_i(t_2)-\overline{n}(t_1)T_i(t_1)]V\approx0.5\pm0.2\ \text{J}, \tag{3}$$

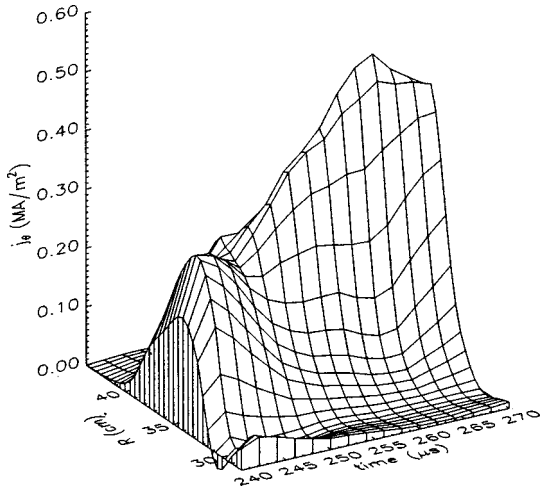

FIG. 12. Surface plot of null-helicity j_θ, which is peaked in the reconnection layer, as a function of radius and time at $Z=0$ cm (from high-resolution 1D probe measurements, averaged over shots 12 233–12 266).

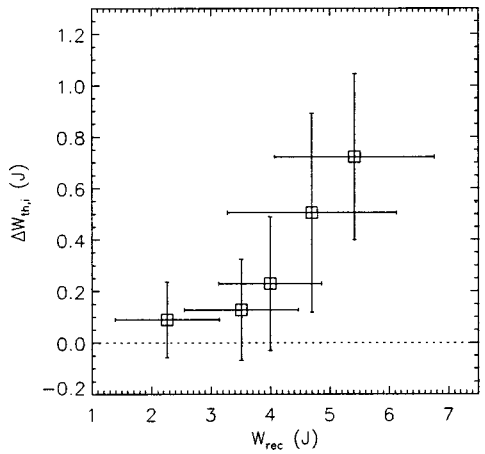

FIG. 13. Observed increase in ion thermal energy $\Delta W_{\mathrm{th},i}$ versus reconnected field energy W_{rec} for null-helicity discharges with varying firing voltages.

where $\overline{n}(t_1)\approx\overline{n}(t_2)\approx 5\pm 1\times 10^{13}$ cm^{-3} is the density averaged over area A, and $T_i(t_1)\approx 6\pm 1$ eV and $T_i(t_2)\approx 13\pm 2$ eV (see Fig. 3). Note that $\Delta W_{\mathrm{th},i}$ is only the *remnant* ion thermal energy in V and does not include ion heat loss during Δt. The rise in ion thermal energy is due predominantly to a rise in T_i, as the density in the layer remains fairly constant ($n_e\approx 5\times 10^{13}$ cm^{-3}) during Δt.

As an aside, an additional set of experiments in which the firing voltage was varied[25] is reported here. A range of $\Delta W_{\mathrm{th},i}$ and W_{rec} were obtained in this experiment. Figure 13 shows that $\Delta W_{\mathrm{th},i}$ scales with W_{rec}, i.e., T_i rises more as more energy is released due to reconnection. Each data point represents the average of five plasma shots at a given firing voltage, and error bars (from data point to extreme) represent one standard deviation in the shot-to-shot scatter. This is consistent with the conclusion from Sec. III that the observed rise in T_i is causally linked to reconnection.

C. Compression

The second term on the LHS of Eq. (1) is a compression term including the work done by pressure forces. It can be estimated approximately as $\langle nT_i(\partial V_R/\partial R+\partial V_Z/\partial Z)\rangle V\Delta t$ (the V_R/R term of $\boldsymbol{\nabla}\cdot\mathbf{V}$ averages to nearly zero over V and is neglected), where the brackets indicate a spatial average over V and temporal average over Δt. Using values of $n\approx 5\pm 1\times 10^{13}$ cm^{-3}, $T_i\approx 10\pm 1$ eV, $\partial V_R/\partial R\approx -(4.8\,\mathrm{km/s})/(0.05\,\mathrm{m})=-9.6\pm 1\times 10^4$ s^{-1}, and $\partial V_Z/\partial Z\approx(8\,\mathrm{km/s})/(0.1\,\mathrm{m})=8\pm 2\times 10^4$ s^{-1}, the compression term is $W_{\mathrm{compression}}\approx -0.16\pm 0.31$ J. The negative value means that there is some ion heating in volume V due to compression. The large relative error arises due to the subtraction of the velocity gradient terms, which results in a small number with large relative error. It will be shown that this compression term is small compared to the ion loss terms, and thus the rough estimate adopted above is justified.

D. Ion energy losses

Since volume V is an open system, a complete ion energy balance must consider ion energy losses due to convective and conductive heat loss. The energy lost must be accounted for since their original source was the dissipated magnetic energy. The heat conduction estimates in this section are based on classical transport. Therefore, they likely represent a lower bound on ion energy loss since the transport is almost certainly not classical. It is important to emphasize that this would only lead to an underestimate of energy conversion to ions. In general, ions may also lose energy to neutrals, and this is discussed.

1. Convection

Convective heat loss, the third term on the LHS of Eq. (1), out of V during Δt can be estimated as the heat convected out of V,

$$W_{\mathrm{out}}\approx[\tfrac{3}{2}n(\mathrm{layer})T_i(\mathrm{layer})]\times(\mathrm{volume\ of\ plasma\ out}), \tag{4}$$

minus the heat convected into V,

$$W_{\mathrm{in}}\approx[\tfrac{3}{2}n(\mathrm{upstream})T_i(\mathrm{upstream})]\times(\mathrm{volume\ of\ plasma\ in}), \tag{5}$$

during Δt. The volumes of plasma flowing out of and into V are determined based on the outflow speed $V_{iZ}\approx 3\pm 0.8$ km/s and inflow speed $V_{iR}\approx 3\pm 0.4$ km/s, respectively. At the boundaries of volume V, the two speeds are approximately equal and thus the volumes convected in and out are also equal (1.4×10^{-2} m^3). The density in the layer n(layer) is approximately $5\pm 1\times 10^{13}$ cm^{-3}, and the average upstream density is approximately $3\pm 0.4\times 10^{13}$ cm^{-3}. The layer T_i is approximately 12 ± 0.9 eV and the average upstream $T_i\approx 10\pm 1.3$ eV. These numbers combine to yield a total ion energy loss due to convection out of volume V during time Δt of $W_{\mathrm{convection}}=W_{\mathrm{out}}-W_{\mathrm{in}}\approx 1.0\pm 0.7$ J.

2. Conduction

Ion heat loss due to thermal conduction is estimated using classical transport. This estimate likely represents a lower bound because (1) T_i gradients may be underestimated due to the time resolution of the measurements, and (2) enhanced nonclassical transport mechanisms are unknown but are likely to exist. Ion energy loss due to classical conduction can be written as[24]

$$\boldsymbol{\nabla}\cdot\mathbf{q}=-\boldsymbol{\nabla}_\perp\cdot(\kappa_\perp\boldsymbol{\nabla}_\perp T_i)-\boldsymbol{\nabla}_\parallel(\kappa_\parallel\boldsymbol{\nabla}_\parallel T_i)+\boldsymbol{\nabla}\cdot\left[\frac{5cnT_i}{2eB}(\mathbf{B}/B\times\boldsymbol{\nabla}T_i)\right], \tag{6}$$

where the last term on the RHS vanishes since ($\mathbf{B}/B\times\boldsymbol{\nabla}T_i$) has only a θ component and $\partial/\partial\theta=0$, and $\kappa_\perp$ and $\kappa_\parallel$ are the perpendicular and parallel ion thermal conductivities, respectively,[24]

$$\kappa_\perp=\frac{2nT_i}{m_i\omega_{ci}^2\tau_i}\approx 2.8\pm 0.6\times 10^{22}\frac{1}{\mathrm{m\,s}}, \tag{7}$$

$$\kappa_\parallel=\frac{3.9nT_i\tau_i}{m_i}\approx 11.0\pm 2.2\times 10^{22}\frac{1}{\mathrm{m\,s}} \tag{8}$$

(T_i in eV and all other variables in cgs units). Average values during Δt have been used: $n=5\pm1\times10^{13}$ cm^{-3}, $T_i=10\pm1$ eV, and $B=250$ G. The total surface area of V is 0.48 m^2, and it is equally divided between being intercepted by B_Z in the perpendicular and parallel directions. Using these values and $\nabla_\perp T_i \approx (2\pm1\text{eV})/(5\text{cm})$ and $\nabla_\parallel T_i \approx (1\pm0.5\text{eV})/(10\ \text{cm})$, the ion heat loss due to classical transport is estimated to be $W_{\text{conduction}} \approx 1.7\pm0.7$ J.

3. Collisions with neutrals

Ion-neutral collisions can be another energy loss channel for heated ions. In MRX regimes, charge exchange is expected to be the dominant ion-neutral interaction. By any reasonable estimate, the plasma inside the current sheet with $T_e>15$ eV should be better than 99% ionized. The rate of He–He$^+$ charge exchange for 10 eV ions is $\langle\sigma v\rangle \approx 4\times10^{-9}$ cm^3/s.[26] The ion density is approximately 5×10^{13} cm^{-3}. A concentration of neutrals equal to 1% of the measured plasma density would result in a charge exchange time of 500 μs, completely negligible on the reconnection time scale of 30 μs. It would take more than a 50% concentration of neutrals in the reconnection layer to bring down the charge exchange time to a more relevant 10 μs. A 50% neutral concentration in the presence of 15 eV electrons is highly unlikely. Therefore, ion energy loss to neutrals is neglected. Note that ion-neutral energy loss would only *increase* the estimate of ion heating due to reconnection.

E. Classical viscous heating

Classical heating per unit volume due to viscosity in the absence of a magnetic field (justified since ions are unmagnetized in the layer) is[24]

$$Q_{\text{vis}} = \eta_0 W_{\alpha\beta} \frac{\partial V_\alpha}{\partial x_\beta}, \tag{9}$$

where $\eta_0 = 0.96 n T_i \tau_i \approx 1.8\times10^{-4}$ J s/m^3 (using $n=5\times10^{13}$ cm^{-3} and $T_i=10$ eV), and the rate-of-strain tensor is given by

$$W_{\alpha\beta} = \frac{\partial V_\alpha}{\partial x_\beta} + \frac{\partial V_\beta}{\partial x_\alpha} - \frac{2}{3}\delta_{\alpha\beta}\nabla\cdot\mathbf{V}. \tag{10}$$

The nonzero velocity gradients averaged over volume V are

$$\frac{\partial V_{iR}}{\partial R} \approx -\frac{4.8\ \text{km/s}}{0.05\ \text{m}} = -9.6\times10^4\ \text{s}^{-1}, \tag{11}$$

$$\frac{\partial V_{iZ}}{\partial Z} \approx \frac{8\ \text{km/s}}{0.1\ \text{m}} = 8.0\times10^4\ \text{s}^{-1}, \tag{12}$$

$$\left|\frac{\partial V_{iZ}}{\partial R}\right| \lesssim \frac{3\ \text{km/s}}{0.05\ \text{m}} = 6.0\times10^4\ \text{s}^{-1}, \tag{13}$$

$$\frac{\partial V_{i\theta}}{\partial R} \lesssim \frac{2\ \text{km/s}}{0.05\ \text{m}} = 4.0\times10^4\ \text{s}^{-1}, \tag{14}$$

where V_{iZ} and $V_{i\theta}$ are based on Mach probe and IDSP measurements, and V_{iR} is based on taking the $E_\theta B_Z$ inflow velocity outside the layer and dividing by the scale length of the layer. Therefore the classical viscous heating per unit volume is

TABLE I. Ion energy budget between $t=245\rightarrow265$ μs in volume V, showing that some 65% of the dissipated magnetic energy W_{rec} is converted to ions W_{ions}.

Process	Energy (J)
W_{rec}	4.8 ± 0.7
Total W_{ions}	3.1 ± 1.0
$\Delta W_{\text{th},i}$	0.5 ± 0.2
$W_{\text{compression}}$	-0.14 ± 0.28
$W_{\text{convection}}$	1.0 ± 0.7
$W_{\text{conduction}}$	$>1.7\pm0.7$
W_{vis}	0.8 ± 0.3

$$Q_{\text{vis}} \approx \eta_0\left(W_{RR}\frac{\partial V_{iR}}{\partial R} + W_{ZZ}\frac{\partial V_{iZ}}{\partial Z} + W_{ZR}\frac{\partial V_{iZ}}{\partial R} + W_{\theta R}\frac{\partial V_{i\theta}}{\partial R}\right) \approx 6.5\pm2.2\times10^6\ \text{J/s m}^3. \tag{15}$$

Using these numbers, the maximum ion energy gained via viscous damping of ion flows is $W_{\text{vis}} \approx Q_{\text{vis}} V \Delta t = 0.8\pm0.3$ J.

Previously in Sec. IV B, it was noted that $V_{i\theta}$ might be underestimated due to limitations in the measurement technique. However, it can be seen from Eq. (15) that increasing $V_{i\theta}$ by a factor of 10 would only increase Q_{vis} (and therefore W_{vis}) by a factor of 1.4. This would not alter the conclusions drawn below that most of the observed ion heating must originate in the nonclassical term Q_{noncl} of Eq. (1).

F. Nonclassical ion heating

The important terms of Eq. (1) are summarized in Table I, which gives a quantitative description of energy conversion to ions based on experimental data. The numbers show that 65 ± 21% of the dissipated field energy is converted to ion energy. Now the question is how much of that energy was converted via nonclassical mechanisms. As mentioned before, classical heating due to ion-electron collisions is neglected due to the long ion-electron energy partition time. In any case, energy available due to ohmic heating is insufficient, estimated to be $\eta_\perp j_\theta^2 V \Delta t \approx 0.2$ J (using $\eta_\perp = 2\times10^{-5}\ \Omega$ m and $j_\theta \sim 0.3$ MA/m^2). Note that this is only 4% of the total dissipated magnetic energy. The other classical mechanism is viscous heating by the ion flow, which was estimated in the preceding section to be 0.8 ± 0.3 J. Subtracting $W_{\text{viscosity}}$ from W_{ions} leaves 2.3 ± 1.0 J of energy which must have been converted to ion energy via nonclassical mechanisms. Thus, 48 ± 21% of the dissipated magnetic energy was converted to ions nonclassically. The various energy components are illustrated in Fig. 14.

In this section, the energy budget of ions was considered carefully. The total energy released due to reconnection was calculated from experimental data and compared to the different components of ion energy, including observable rise in ion thermal energy and ion heat loss due to convection and conduction. The energy budget showed that some 48% of the

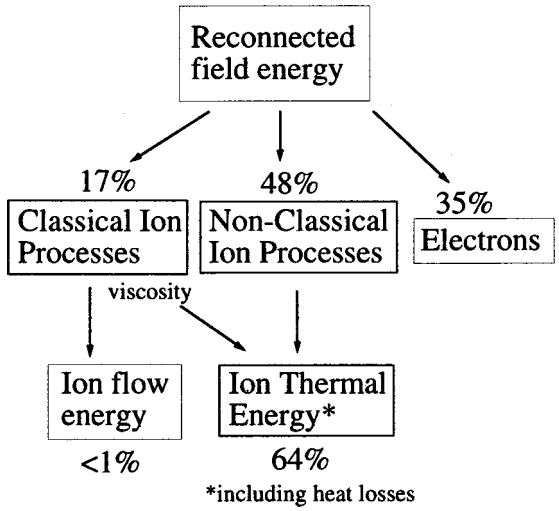

FIG. 14. Illustration of the field and ion energy budget for null-helicity reconnection. Ions gained 65% of the dissipated field energy, and 48% of the dissipated field energy was converted nonclassically.

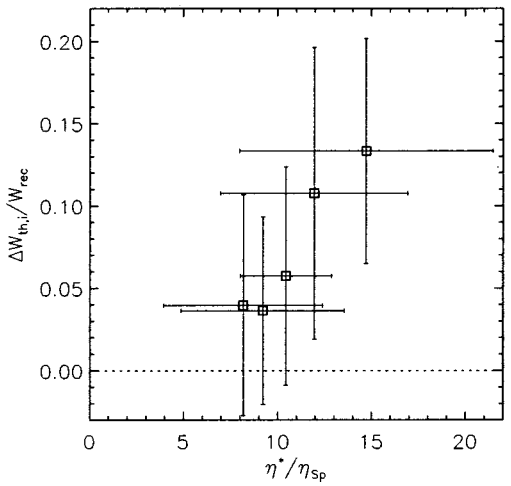

FIG. 15. Increase in ion thermal energy normalized by reconnected field energy for varying resistivity enhancement factors (null-helicity), showing a correlation between the two.

dissipated magnetic energy was converted to ions nonclassically. This finding on nonclassical ion heating during reconnection, based on experimental measurements, has significant implications since the basic mechanisms responsible for enhanced reconnection rates and energy conversion are still poorly understood.

VI. DISCUSSION

A. Correlation of ion heating with "resistivity enhancement"

In the preceding section, it was established that ions are heated via nonclassical dissipation mechanisms. In this section, experimental data is given suggesting a correlation between ion heating and resistivity enhancement for the null-helicity case. Resistivity enhancement is defined as the ratio of the measured plasma resistivity η^* to the classical Spitzer resistivity $\eta_{Sp}=\eta_\perp$. The relative importance of nonclassical versus classical dissipation is embodied in the enhancement factor η^*/η_{Sp}, which has been shown to increase as collisionality decreases.[11] One possible explanation for this effect is that as the plasma becomes more collisionless, wave fields can scatter current-carrying particles, increasing η^*, while also heating the ions (e.g., via Landau resonance).

By scanning the discharge voltage[25] in a set of null-helicity experiments, $\Delta W_{th,i}/W_{rec}$ and η^*/η_{Sp} are varied. Increasing the discharge voltage increases reconnection and thus increases ion heating. The scaling of the quantities with each other can provide insight into the nature of the nonclassical ion heating mechanisms. Shown in Fig. 15 is $\Delta W_{th,i}/W_{rec}$ versus η^*/η_{Sp}. The fraction $\Delta W_{th,i}/W_{rec}$ increases from approximately 4% to 14% as η^*/η_{Sp} increases from 8 to 15, as shown in Fig. 15. (Note again that $\Delta W_{th,i}$ is not the total energy gained by ions but only the remnant ion thermal energy in volume V not including ion heat loss.) Although the error bars are sizable, the trend between the energy converted to ions and the resistivity enhancement is clear. The subtle, and perhaps unexpected, hint provided by Fig. 15 is that the (nonclassical) mechanism determining the enhanced reconnection rate (and hence increased reconnected field energy) may also be responsible for channeling the reconnected field energy to the ions. The details, however, would also depend on the ion heat loss characteristics.

B. Possible ion heating mechanisms

The experimental data have indicated the existence of nonclassical ion heating, nonclassical resistivity, and possibly a correlation between the two. The obvious next step experimentally, presently underway, is to investigate the frequency spectrum of turbulent fluctuations with the possibility of identifying relevant modes which can explain the enhanced resistivity and possibly also the ion heating. Theoretically, much effort has been devoted to addressing these issues and a full review is beyond the scope of this paper.[27] Two approaches which might account for the enhanced resistivity and ion heating are described below.

There are several free energy sources in the MRX current sheet which can drive unstable fluctuations, including a large density gradient and cross field current. Turbulence driven by unstable modes could provide a mechanism to produce resistivity and ion heating in current sheets. One instability which has been extensively investigated theoretically in the context of current sheets is the lower-hybrid drift instability.[28,7] It is a high frequency ($\Omega_i \ll \omega \ll \Omega_e$) mode driven unstable by cross-field current and associated density gradients, and it persists in the regime $T_e \lesssim T_i$ as required in MRX. The mode is strongly growing in ρ_i-scale density gradients and has a wavelength near the electron gyroradius and a phase velocity near the ion thermal speed. The value of the phase velocity allows for the possibility of resonant interaction with and heating of the ion population in the MRX current sheet. It is well known that the mode is linearly stabilized at high plasma β (Ref. 29) and should exist with appreciable amplitude only at the edges of the current sheet, while nonclassical resistivity and ion heating are seen in the center of the MRX current sheet. However, strong radial

transport produced by this mode could result in enhanced resistivity.[7] Measurements of fluctuations in MRX show the presence of strong fluctuations in the lower-hybrid frequency range at the edges of the current sheet, and dispersion of these fluctuations is consistent with the lower-hybrid drift mode.[23] Studies of the relationships of these modes to the reconnection process are currently underway.

Another possible ion heating mechanism manifests itself in collisionless reconnection simulations based on a 2.5-D hybrid code (kinetic ions, fluid electrons) which includes Hall dynamics and electron inertia.[8] In this simulation, a two-scale structure develops in the reconnection layer owing to the Hall effect, which allows ions and electrons to decouple on scale lengths shorter than c/ω_{pi}, the scale at which ions become unmagnetized. (MRX data also show a current sheet thickness of c/ω_{pi}.) The electrons continue inward into the layer until the c/ω_{pe} scale at which they finally become unmagnetized and the flux-freezing constraint is finally broken. A self-consistent electric field arises between the c/ω_{pi} and c/ω_{pe} scales due to the charge separation and can accelerate inflowing ions up to the Alfvén speed. The counter-streaming ions which come in from both sides of the layer mix and can appear to be heated instantaneously. This would seem to be consistent with the immediate rise in T_i observed in the center of the reconnection layer in MRX. However, when 3D effects are included in the simulations, the thin electron layer breaks up turbulently,[30] and it is not clear if this ion heating mechanism would survive in a physical reconnection layer. Furthermore, the simulations are collisionless and may not model accurately the dominant dissipation processes in the MRX reconnection layer. Although experimental measurements of E_R and V_{iR} on MRX do not reveal the two-scale structure described above, the theory cannot be ruled out due to spatial limitations in the measurements. A more precise electrostatic probe array will be utilized to address this issue.

VII. SUMMARY

In this work, local ion temperature was measured in a well-characterized reconnection layer. A rise in T_i during reconnection was identified, for both null-helicity ($6\rightarrow 17$ eV) and co-helicity ($3\rightarrow 7$ eV) reconnection. Furthermore, the T_i rise was found to be causally linked to the reconnection process, i.e., the T_i rise occurred only when reconnection was driven, and the magnitude of the rise scales with the magnetic field energy dissipated. Additionally, the rise in T_i was shown to be localized spatially in the region of the reconnection current sheet and magnetic field reversal. These results collectively could be interpreted as the first clear experimental demonstration of ion heating due to magnetic reconnection.

Local downstream ion flow measurements showed the flows to be small, at most 25% of V_A ($0.25V_A \approx 8$ km/s). This observation is consistent with the high downstream pressure observed in MRX, postulated to arise due to fast pressure equalization in the finite downstream volume. The small flow speeds of MRX are in direct contrast to the results of TS-3[9] and SSX,[10] as well as to classical MHD reconnection theories which ignore the effects of downstream pressure. Toroidal flows were also measured and shown to be small (a few km/s at most) and not a possible energy source for the observed ion heating.

An ion energy balance for the reconnected field and ion energy showed that substantial ion heating occurred and that approximately 65% of the reconnected field energy was converted to ion thermal energy. At most, 17% of the dissipated field energy would have been converted to ion energy via classical viscosity, meaning that 48% of the energy was converted nonclassically. Finally, there is a hint of stronger ion heating with increased resistivity enhancement, suggesting a relationship between the nonclassical mechanisms responsible for enhanced resistivity and ion heating.

The exact mechanism(s) for the heating and associated ''anomalous'' resistivity is still an open question and the subject of ongoing research, both experimentally and theoretically. Conversely, the identification of nonclassical ion heating on MRX should impact current thinking on the possible nonclassical micro-physics in the reconnection layer.

ACKNOWLEDGMENTS

This work was taken from the doctoral dissertation of S. Hsu. It is a pleasure to acknowledge D. Cylinder for technical assistance and Dr. F. Trintchouk, Dr. F. Levinton, and Dr. R. Bell for helpful discussions regarding the spectroscopy. MRX is funded jointly by the Dept. of Energy, the National Aeronautics and Space Administration (NASA), and the National Science Foundation. Two of us (S.C.H. and T.A.C.) acknowledge the support of NASA Graduate Student Researchers Program fellowships.

APPENDIX: MACH PROBE DATA ANALYSIS

A Mach probe collects ion saturation current I_{sat} on each of two oppositely facing electrodes. Intuitively, it is reasonable to expect that the difference between the collected currents should reveal information about the average ion drift speed V_i past the probe. The experimental quantity measured is

$$K \equiv \frac{I_+ - I_-}{I_+ + I_-}, \tag{A1}$$

where I_+ and I_- are the (ion saturation) currents collected by the upstream and downstream electrodes, respectively. By considering the appropriate probe sheath physics, a theoretical relationship between K and V_i can be postulated.

A large number of Mach probe papers exist in the literature,[15,31] and a review of them will not be attempted here. The important parameters to consider are a/λ_D, T_i/T_e, and ρ_i/a, where a is the characteristic probe electrode dimension and λ_D is the Debye length. MRX plasma and Mach probe parameters fall into the regime $a/\lambda_D \gg 1$, $T_i \gtrsim T_e$, and $\rho_i/a \gg 1$, in which there is no general, rigorous theory to predict I_{sat}. However, the model of Hudis and Lidsky[15] can be used as a starting point. This model is based on the Bohm sheath model,[32] in which $T_i \ll T_e$, but modified

to include a net ion drift V_i [$<C_s \equiv \sqrt{(T_e+T_i)/m_i}$] at the sheath edge. The ion saturation current in this case can be approximated by

$$I_{\pm} = \exp(-1/2) n_{i0} e A C_s \exp\left(\frac{m_i V_i^2}{2T_e}\right) \exp\left(\pm \frac{\sqrt{m_i T_i} V_i}{T_e}\right), \tag{A2}$$

where n_{i0} is the density far from the probe and A is the electrode surface area. Numerical solutions[33] for I_{sat} have shown that the Bohm sheath model is not strongly dependent on T_i for $T_i \lesssim T_e$. Since $T_i \sim T_e$ in the experiments for which ion flow speeds are measured, Eq. (A2) can still be used. Substituting $I_{\pm}$ into Eq. (A1) yields

$$V_i = \sqrt{\frac{T_e}{T_i}} \sqrt{\frac{T_e}{m_i}} \tanh^{-1} K. \tag{A3}$$

It must be emphasized that, as a general rule, theoretical expressions for electrostatic probes such as Eq. (A3) are usually not accurate to better than a factor of 2. This is not surprising given the nonrigorous justifications relied upon in the above discussion. The trends (spatial profile and temporal evolution) which are measured, however, are still meaningful. Ideally, the absolute value of Mach probe results should be calibrated with an independent measurement. It is found that Mach probe measurements based on Eq. (A3) agree with Doppler shifts of ions obtained by spectroscopy to better than 50%.[4] Thus, V_i values reported in this paper are based on Eq. (A3) but include an empirical calibration factor of 0.75.

[1] V. M. Vasyliunas, Rev. Geophys. Space Phys. **13**, 303 (1975); D. Biskamp, Phys. Rep. **237**, 179 (1994).

[2] M. Yamada, H. Ji, S. Hsu, T. Carter, R. Kulsrud, N. Bretz, F. Jobes, Y. Ono, and F. Perkins, Phys. Plasmas **4**, 1936 (1997); M. Yamada, H. Ji, S. Hsu, T. Carter, R. Kulsrud, Y. Ono, and F. Perkins, Phys. Rev. Lett. **78**, 3117 (1997).

[3] S. C. Hsu, G. Fiksel, T. A. Carter, H. Ji, R. M. Kulsrud, and M. Yamada, Phys. Rev. Lett. **84**, 3859 (2000).

[4] S. C. Hsu, Ph.D. thesis, Princeton University, 2000.

[5] G. Fiksel, D. J. D. Hartog, and P. W. Fontana, Rev. Sci. Instrum. **69**, 2024 (1998).

[6] P. A. Sweet, in *Electromagnetic Phenomena in Cosmical Physics*, edited by B. Lehnert (Cambridge University Press, New York, 1958), pp. 123–134; E. N. Parker, J. Geophys. Res. **62**, 509 (1957).

[7] J. D. Huba, J. F. Drake, and N. T. Gladd, Phys. Fluids **23**, 552 (1980).

[8] M. A. Shay, J. F. Drake, R. E. Denton, and D. Biskamp, J. Geophys. Res. **103**, 9165 (1998).

[9] Y. Ono, M. Yamada, T. Akao, T. Tajima, and R. Matsumoto, Phys. Rev. Lett. **76**, 3328 (1996).

[10] T. W. Kornack, P. K. Sollins, and M. R. Brown, Phys. Rev. E **58**, R36 (1998).

[11] H. Ji, M. Yamada, S. Hsu, and R. Kulsrud, Phys. Rev. Lett. **80**, 3256 (1998); H. Ji, M. Yamada, S. Hsu, R. Kulsrud, T. Carter, and S. Zaharia, Phys. Plasmas **6**, 1743 (1999).

[12] M. Yamada, H. Ji, S. Hsu, T. Carter, R. Kulsrud, and F. Trintchouk, Phys. Plasmas **7**, 1781 (2000).

[13] E. G. Harris, Nuovo Cimento **23**, 115 (1962).

[14] Toroidal symmetry has been checked by rotating a magnetic probe array over several θ positions. No evidence of gross asymmetry was found, thus justifying the assumption of toroidal symmetry and the calculations of ψ and E_θ based on B_Z.

[15] M. Hudis and L. M. Lidsky, J. Appl. Phys. **41**, 5011 (1970).

[16] TF/PF bank voltages=13/11 kV; TF/PF bank capacitances=120 μF; TF/PF trigger=180/270 μs; TF/PF crowbar (w/reconnection)=270/290 μs; TF/PF crowbar (w/o reconnection): 270/220 (null-helicity), 270/200 (co-helicity); initial He gas pressure=6 mT.

[17] During plasma formation, coil current is increasing and private flux is reconnected into public flux, establishing a reconnection layer elongated in the R direction. This is push reconnection.

[18] Negative values of E_θ and j_θ before $t \approx 248$ μs for co-helicity are due to the end of the push reconnection phase in which the induced E_θ is in the other direction. The negative E_θ after $t=270$ μs is likely due to the plasma pinching off from one flux-core.

[19] M. Yamada, Y. Ono, A. Hayakawa, and M. Katsurai, Phys. Rev. Lett. **65**, 721 (1990).

[20] High downstream pressure may arise due to pressure equalization along field lines which connect the reconnection region to the downstream regions near the flux cores. The thermal transit time of 15 eV electrons along this path is ~ 1 μs, meaning that buildup of downstream pressure due to recirculating electrons over 20–30 μs is plausible.

[21] Preliminary floating potential measurements suggest an E_R which would give rise to an $E_R \times B_Z$ drift on the order of 30 km/s.

[22] T. W. Speiser, J. Geophys. Res. **70**, 4219 (1965).

[23] T. Carter, F. Trintchouk, H. Ji, R. Kulsrud, and M. Yamada, Bull. Am. Phys. Soc. **45**, 270 (2000).

[24] S. I. Braginskii, in *Reviews of Plasma Physics*, edited by M. A. Leontovich (Consultants Bureau, New York, 1965), Vol. 1, pp. 205–311.

[25] TF/PF bank voltages=11/9, 12/10, 12.5/10.5, 13/11, 14/12 kV.

[26] R. K. Janev, W. D. Langer, K. Evans, and D. E. Post, *Elementary Processes in Hydrogen-Helium Plasmas* (Springer-Verlag, New York, 1987).

[27] F. V. Coroniti, J. Geophys. Res. **90**, 7427 (1985).

[28] R. C. Davidson and N. T. Gladd, Phys. Fluids **18**, 1327 (1975).

[29] R. C. Davidson, N. T. Gladd, C. S. Wu, and J. D. Huba, Phys. Rev. Lett. **37**, 750 (1975).

[30] J. F. Drake, D. Biskamp, and A. Zeiler, Geophys. Res. Lett. **24**, 2921 (1997).

[31] P. C. Stangeby, Phys. Fluids **27**, 2699 (1984); K. S. Chung, J. Appl. Phys. **69**, 3451 (1990); B. J. Peterson, J. N. Talmadge, D. T. Anderson, F. S. B. Anderson, and J. L. Shobet, Rev. Sci. Instrum. **65**, 2599 (1994).

[32] D. Bohm, E. H. S. Burshop, and H. S. W. Massey, in *The Characteristics of Electrical Discharges in Magnetic Fields*, edited by A. Guthrie and R. K. Wakerling (McGraw-Hill, New York, 1949), pp. 13–76.

[33] See National Technical Information Service document (J. G. Laframboise, ''Theory of Spherical and Cylindrical Probes in a Collisionless Maxwellian Plasma at Rest,'' UTIAS **100**, 1966). Copies may be ordered from NTIS, Springfield, VA 22161.